



## **Fundamental Science of Energy 010**

### **"Fundamental studies of diffusion and reactions in hydrogen storage materials"**

**Chris G. Van de Walle, Amra Peles,  
Anderson Janotti, and Gareth B. Wilson-Short**

**October 2008**

This paper is part of the University of California Energy Institute's (UCEI) Fundamental Science of Energy Working Paper Series. UCEI is a multi-campus research unit of the University of California located on the Berkeley campus.

UC Energy Institute  
2547 Channing Way, # 5180  
Berkeley, California 94720-5180  
[www.ucei.berkeley.edu](http://www.ucei.berkeley.edu)

This report was issued in order to disseminate results of and information about energy research at the University of California campuses. Any conclusions or opinions expressed are those of the authors and not necessarily those of the Regents of the University of California, the University of California Energy Institute or the sponsors of the research. Readers with further interest in or questions about the subject matter of the report are encouraged to contact the authors directly.



## UCEI Working Paper – Fundamental Science of Energy

# Fundamental studies of diffusion and reactions in hydrogen storage materials

**Chris G. Van de Walle, Amra Peles<sup>\*</sup>, Anderson Janotti, and Gareth Wilson-Short**

Materials Department, University of California, Santa Barbara  
[vandewalle@mrl.ucsb.edu](mailto:vandewalle@mrl.ucsb.edu)

### Abstract

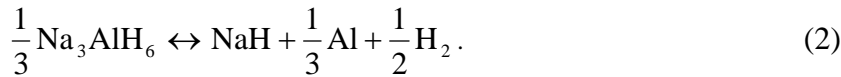
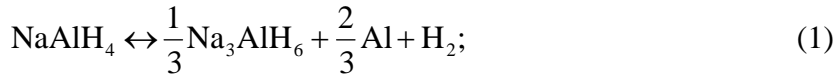
Hydrogen can serve as an energy carrier in a carbon-neutral system of energy production and use [1,2], but adequate hydrogen storage materials are still lacking in spite of many decades of investigations. In addition to being reversible and meeting stringent weight % and volume criteria, candidate materials must exhibit favourable kinetics for hydrogen uptake and release. The fundamental mechanisms of the (de)hydrogenation process have remained elusive to date. We have initiated a study of the relevant reactions, resulting in an identification of the dominant defect species involved in hydrogen transport in non-metallic hosts. While the concepts discussed here are general, we illustrate them with detailed first-principles results for sodium alanate. We identify hydrogen-related point defects as the essential mediators of hydrogen transport. A novel finding of this work is that the defects are positively or negatively charged, and hence their formation energies are Fermi-level dependent—an important feature that has not been recognized in past studies. This dependence enables us to explain why small amounts of transition-metal additives drastically alter the kinetics of dehydrogenation.

---

<sup>\*</sup> Present address: United Technologies Research Center, 411 Silver Lane, MS 129-90, East Hartford, CT 06108

## 1. Introduction

Complex hydrides of light elements are attractive as storage materials due to the high hydrogen content and the demonstrated cycling capability. In  $\text{NaAlH}_4$  hydrogen release and uptake is accomplished through a sequence of chemical reactions:



The hydrogen gravimetric capacity for these reactions is 5.6 wt%. However, in pure  $\text{NaAlH}_4$  both reactions are slow and proceed only at temperatures too high for practical applications. In 1997 it was discovered that addition of small amounts of transition metals, such as Ti or Zr, drastically enhances the kinetics and allows cycling at temperatures and pressures that are close to optimal [3]. A fundamental explanation of these phenomena would clearly provide highly needed guidance in the optimization of existing and the design of novel storage materials [4-11].

Crystal defects are known to play a role in chemical reactions and their presence profoundly affects diffusion and mass transport in materials [12]. It therefore is logical to assume that this will also be the case in hydrogen storage materials. First-principles calculations based on density functional theory have played an important role in elucidating the physics of point defects in other materials [13,14]; we therefore set out to apply this methodology to hydrogen storage materials. We have performed density functional calculations of the *creation* of hydrogen-related point defects in  $\text{NaAlH}_4$  and their *diffusion* through the material, enabling us to identify the point defects that play a decisive role in the (de)hydrogenation reactions.

An important feature of these defects is that they are *charged*, and therefore their formation energy and concentration is strongly affected by the presence of electrically active extrinsic impurities in the material. Our studies show that this provides a consistent explanation for the effect of transition-metal impurities (such as Ti and Zr) on hydrogen kinetics, and can reconcile a variety of seemingly conflicting results that have appeared in the literature [4-11, 15-17]. The hydrogen-related point defects also induce significant rearrangements of the local lattice of the host, thereby providing nucleation sites for reaction (1).

## 2. Methodology

In thermodynamic equilibrium the concentration  $c(X)$  of a point defect  $X$  at temperature  $T$  is given by

$$c(X) = N \exp\left[\frac{E_f(X)}{kT}\right] \quad (3)$$

where  $N$  represents the total number of sites on which the defect can be incorporated and  $E_f$  is the formation energy of the defect, defined as [18]

$$E_f(X^q) = E_{tot}(X^q) - E_{tot}(bulk) - \sum_i n_i \mu_i + q\mu_e. \quad (4)$$

Here  $E_{tot}(X^q)$  and  $E_{tot}(bulk)$  denote total energies of a supercell containing the defect in charge state  $q$  and of a supercell containing perfect bulk NaAlH<sub>4</sub>.  $\mu_i$  is the chemical potential of species  $i$ , i.e., the energy of the reservoir with which atomic species  $i$  is exchanged, and  $n_i$  denotes the number of atoms of species  $i$  that have been added ( $n_i > 0$ ) or removed ( $n_i < 0$ ) to create the defect.  $\mu_e$  represents the energy of electrons in the charge reservoir, i.e., the electron chemical potential or *Fermi energy* (referenced to the top of

the valence band).  $E_f$  is, in principle, a *free energy*; however, at the temperatures of interest the effects of pressure (except for gaseous phases) and vibrational entropy [19] do not affect our conclusions.

The first principles calculations are based on density functional theory using the generalized gradient approximation [20] and the projector augmented wave method [21] as implemented in the VASP *ab-initio* simulation package [22]. The calculations were performed in a supercell containing 96 atoms, with an energy cutoff of 450 eV and a 2x2x2 special k-point mesh. Our calculated band gap for NaAlH<sub>4</sub> is 4.75 eV. An experimental value of the band gap has not been reported, but density functional theory is known to underestimate the gap; quasiparticle calculations suggest a band gap of 6.9 eV [23]. Migration barriers were calculated using the Nudged Elastic Band method [24].

### 3. Results

#### 3.a. Energetics

Sodium alanate is an ionic compound consisting of sodium cations (Na<sup>+</sup>) and covalently bonded anion complexes (AlH<sub>4</sub><sup>-</sup>) situated on tetragonal-symmetry sites with a I4<sub>1</sub>/a crystallographic space group. Figure 1 shows a schematic of the structure. The chemical bonding in NaAlH<sub>4</sub> can be most easily understood by considering it as an ionic compound in which Na<sup>+</sup> ions are the cations and (AlH<sub>4</sub>)<sup>-</sup> units act as anions. Within the (AlH<sub>4</sub>)<sup>-</sup> units, the bonding between Al and H has significant covalent character. Al has three valence electrons, and hence would normally bond only to three H atoms. A fourth H atom can be added, provided an extra electron is available to complete the two-electron bond; hence the negative charge on the (AlH<sub>4</sub>)<sup>-</sup> unit.

Our calculated formation energies for the most relevant intrinsic defects in NaAlH<sub>4</sub>, namely hydrogen interstitials (H<sub>i</sub>) and hydrogen vacancies (V<sub>H</sub>) in three possible charge states (+1,0,-1), are shown in Fig. 2. In both cases, charged defects are energetically more favourable than neutral states over the entire range of Fermi-level values. Such behavior is characteristic of systems with negative correlation energy  $U$ , and usually occurs in conjunction with large lattice relaxations [25], as discussed below.

The concentrations of charged defects are not independent but coupled by the condition of charge neutrality

$$\sum_j q_j c(X_j^{q_j}) - n + p = 0. \quad (5)$$

The first term is a sum over all defects  $X_j^{q_j}$  in charge state  $q_j$ ,  $n$  is the concentration of electrons in the conduction band, and  $p$  is the concentration of holes in valence band. In an insulator such as NaAlH<sub>4</sub> the concentrations of free carriers  $n$  and  $p$  are very small, and therefore charge neutrality is accomplished by incorporation of defects with opposite charge. The relevant point defects and impurities introduce defect levels that are deep in the band gap, causing the resulting Fermi-level positions to be far from the band edges and justifying the neglect of  $n$  and  $p$  in equation (5). The defects with the lowest formation energy have the highest concentrations and dominate in equation (5). Figure 2 therefore indicates that, in the absence of extrinsic impurities, the Fermi level will have the value  $\mu_e^{\text{int}}=2.97$  eV where the formation energies of  $V_H^+$  and  $H_i^-$  are equal. At this position of  $E_F$ , the formation energy of these defects is 0.81 eV. Using Eq. (3), this corresponds to a concentration of only about  $10^{11}$  cm<sup>-3</sup> at 100 °C. Such a low concentration of defects does not lead to any observable effects on the properties of the material.

So why does the incorporation of extrinsic impurities such as Ti or Zr affect the kinetics? For these impurities, we have explored both substitutional and interstitial configurations. The lowest formation energies were obtained for the impurity substituting on an Al site; the preference over the Na site is consistent with the chemical similarity of these transition-metal impurities with Al, and also with recent x-ray diffraction results [9]. Figure 3 shows that  $\text{Ti}_{\text{Al}}$  also acts as a “negative- $U$ ” center. The Fermi-level position where positive and negative charge states have equal formation energies determines the *transition level*  $\varepsilon(+/-)$  [18]. If  $\text{Ti}_{\text{Al}}$  is present in concentrations exceeding those of other charged defects, the Fermi level will be pinned at  $\mu_e = \varepsilon(+/-) = 3.41$  eV. This is true irrespective of whether  $\text{Ti}_{\text{Al}}$  is incorporated under equilibrium or non-equilibrium conditions (including processes such as ball milling [15]), since it is driven by equilibration of electronic states for Ti at a single site.

Incorporation of an electrically active defect such as Ti therefore has the important effect of shifting the Fermi level from its value in intrinsic material, in this case by an amount  $\Delta\mu_e = \varepsilon(+/-) - \mu_e^{\text{int}} = 0.44$  eV. This shift lowers the formation energy  $E_f$  of the predominant hydrogen-related point defect ( $\text{H}_i^-$ ) by  $\Delta E_f = 0.44$  eV. This decrease in  $E_f$  causes an increase in the concentration of the defect, resulting in an increase in self-diffusion. The kinetics of hydrogen-related point defects is intimately tied to the decomposition reaction (1), and a lowering of  $E_f$  allows achieving a given concentration of defects at a lower temperature; experimentally, Ti-induced decreases of the decomposition temperature  $\Delta T \approx 60$  °C [3] and  $\Delta T \approx 100$  °C [26] have been reported. Using Eq. (3), we also find that the decrease  $\Delta E_f = 0.44$  eV at a given temperature results in an increase of the defect concentration by six orders of magnitude! The defect concentrations can rise to about  $10^{17}$  cm<sup>-3</sup>, which (in combination with the low migration barriers discussed below) is more than adequate to cause copious amounts of self-diffusion. At the same time, such concentrations are small enough to fulfil the condition that the hydrogen-

related defects have no effect on the Fermi-level position in the presence of an extrinsic impurity. Indeed,  $\text{Ti}_{\text{Al}}$  concentrations well exceeding  $10^{17} \text{ cm}^{-3}$  should be easily attainable in doped material, given that typically several mol % of Ti are added (corresponding to concentrations above  $10^{20} \text{ cm}^{-3}$ ). In fact, our findings emphasize that only a small fraction of this added Ti is needed to achieve the desired effect. This is good news from the point of view of technological applications, since adding large amounts of Ti adversely affects the hydrogen weight capacity.

Since the kinetics of hydrogen-related point defects is intimately tied to the decomposition reaction (1) we expect that our calculated decrease  $\Delta\mu_e$  in the activation energy for hydrogen diffusion would be reflected in the experimentally observed change in activation energy  $\Delta Q$  for Ti-doped alanate compared to pure alanate.  $\Delta\mu_e=0.44 \text{ eV}$  corresponds to  $42 \text{ kJ/mol}$ , in very good agreement with reported values ( $\sim 40 \text{ kJ}/(\text{mol H}_2)$ ) [27]. The observed lowering was independent of the amount of added Ti, consistent with our statement that as long as the  $\text{Ti}_{\text{Al}}$  concentration exceeds the concentration of hydrogen-related defects, the Fermi level will be pinned at the  $\varepsilon(+/-)$  transition level, irrespective of the Ti concentration.

The results presented in Fig. 2 demonstrate that a similar mechanism applies in the case of Zr doping. Zr also exhibits negative- $U$  behaviour and the Fermi level is pinned at  $\varepsilon(+/-)=2.90 \text{ eV}$ . The Zr-induced shift in the Fermi level ( $\Delta\mu_e=-0.07 \text{ eV}$ ) and hence in  $E_f$  is much smaller than in the case of Ti, resulting in a much smaller impact on reaction kinetics. An experimental comparison of Ti- and Zr-doped alanate indeed suggested a change in the activation enthalpy between Ti- and Zr-doped samples of  $30 \text{ kJ/mol}$  [28]. Combined with the result for Ti cited above this implies an enhancement of only  $\sim 12 \text{ kJ/mol}$  over the value of undoped alanate, consistent with our estimated value of  $0.07 \text{ eV}$  or  $\sim 7 \text{ kJ/mol}$ .

### 3.b. Atomic structure

The hydrogen-related defects also induce remarkable changes in lattice geometry, as illustrated in Figs. 4-7. To facilitate the visualization, we use the same view as for the atomic positions in the perfect crystal (Fig. 1). Figure 4 shows that the hydrogen vacancy in the positive charge state leads to a significant rearrangement of the surrounding lattice. The driving force for this rearrangement can be understood as follows. As noted above,  $(\text{AlH}_4)^-$  units in the perfect  $\text{NaAlH}_4$  lattice need to acquire a negative charge in order to be able to form *four* Al-H bonds with two electrons each. This fourfold coordination also determines the tetrahedral geometry of these units, corresponding to  $sp^3$  hybridization of the Al atom. When a hydrogen atom is removed (i.e., a hydrogen vacancy is created), the resulting  $\text{AlH}_3$  unit no longer needs the extra electron (explaining why the vacancy becomes positively charged, at least when the Fermi level is low enough to easily accept this electron). In addition, the driving force for tetrahedral coordination disappears, and  $\text{AlH}_3$  assumes its usual planar geometry, characterized by  $sp^2$  hybridization of the Al, with an empty Al  $p_z$  orbital pointing out of the plane of the  $\text{AlH}_3$ . It is the presence of this  $p_z$  orbital that is likely responsible for a further lattice rearrangement, which actually turns a neighboring  $(\text{AlH}_4)^-$  unit into a planar  $\text{AlH}_3$  plus an interstitial H atom. This latter H is almost symmetrically located between the two  $\text{AlH}_3$  units; indeed the distances between this H atom and the neighboring Al atoms are 1.70 and 1.85 Å. The distances between the central H atom and the H atoms in the  $\text{AlH}_3$  units are 2.65, 2.59, and 2.58 Å for the first unit, and 2.49, 2.52, and 2.60 Å for the second unit.

The geometry of  $V_{\text{H}}^-$  (shown in Fig. 6) is relatively simple. A hydrogen is removed from an  $(\text{AlH}_4)^-$  unit, and an additional electron added. This leaves an Al atom surrounded by three H atoms and a “dangling bond” filled with two electrons.  $s^2p^3$  hybridization becomes more favorable, with the Al-H bond angles becoming closer to  $90^\circ$  (the calculated angles range from  $95$  to  $98^\circ$ , compared with angles of  $107$  and  $114^\circ$  in

bulk  $\text{AlH}_4$ ). The  $V_{\text{H}}^-$  defect has a doubly occupied state in the band gap; Fig.6 shows an isosurface of the charge density associated with this defect state, clearly demonstrating its “dangling-bond” character.

The geometry of a hydrogen interstitial in the positive charge state, depicted in Fig. 6, is probably the most surprising. This extra hydrogen atom does not simply move into an interstitial site in the lattice; in fact, it creates a large rearrangement involving at least 10 host atoms. The final geometry can be considered to consist of a hydrogen vacancy in the positive charge state, as described above (with atomic positions that agree with those reported above to within 0.01 Å) plus an interstitial  $\text{H}_2$  molecule. I.e., the presence of the interstitial induces the crystal to make another interstitial H available, with which the first interstitial can bind and form  $\text{H}_2$ . The energy gained in the process of molecule formation apparently exceeds the cost of creating the additional vacancy. This energy gain can be understood in terms of destabilization of an  $(\text{AlH}_4)^-$  unit in the presence of a proton. An additional proton in the lattice is attracted to the negatively charged complex. Next, electron transfer to the proton may occur, leaving a neutral  $(\text{AlH}_4)^0$ , which is known to be an unstable species. Alternatively, proton transfer to  $(\text{AlH}_4)^-$  may occur, which results in  $\text{AlH}_5$ , also known to be unstable. Either way, spontaneous decomposition of the  $\text{AlH}_4$  or  $\text{AlH}_5$  will occur, resulting in the stable species  $\text{H}_2$  and  $\text{AlH}_3$ . The latter can be regarded as a missing hydrogen and electron, i.e., a positively charged vacancy. Based on this picture, one might suspect that the formation energy of  $\text{H}_i^+$  would be the sum of the formation energies of  $V_{\text{H}}^+$  and an interstitial molecule,  $(\text{H}_2)_i$ . We have therefore also calculated the formation energy of  $(\text{H}_2)_i$ , and it turns out to be significantly larger (by about 0.7 eV) than the difference in formation energies of  $\text{H}_i^+$  and  $V_{\text{H}}^+$ ; this indicates that the interstitial molecule significantly lowers its energy due to its proximity to the vacancy, presumably because additional space in the lattice is available.

Figure 7, finally, shows the geometry of a negatively charged hydrogen interstitial. The additional hydrogen is located more or less symmetrically between two  $(\text{AlH}_4)^-$  units. The distances between this additional H atom and the neighboring Al atoms are 1.78 and 1.84 Å. The distances to the closest H atoms are all larger than 2.23 Å. The  $\text{H}_i^-$  defect induces two states in the band gap: one very close to the valence-band maximum, which is valence-band like with density on the H atoms, the other at  $\sim 1.3$  eV above the valence-band maximum, which is plotted in Fig. 7.

Figures 4-7 clearly illustrate that all of the defects induce significant modifications of one or more surrounding  $\text{AlH}_4^-$  complexes, which in pure alanate exhibit close to tetrahedral geometry. Changes in the coordination number of Al and H atoms as well as in the symmetry of the resulting Al-H complexes are observed. We speculate that these distortions can serve as nuclei for the formation of new phases, which is necessary for reaction (1).

### 3.c. Diffusion

We also addressed the mobility of the defects. For  $\text{H}_i^-$  we calculated a migration barrier (i.e., the energy difference between the saddle point and the ground state)  $E_m=0.22$  eV. For  $V_{\text{H}}^+$ , the path was calculated by moving a hydrogen atom from a nearby  $\text{AlH}_4$  complex into the vacancy, resulting in  $E_m=0.26$  eV. The diffusion coefficient is given by  $D=D_0 \exp(-E_m/kT)$ , with  $D_0 \approx 0.07 \text{ cm}^2/\text{s}$  based on the vibrational frequency and the jump length [18]. Once formed, these defects are therefore highly mobile and can easily traverse macroscopic distances at temperatures below room temperature. These results agree well with the observation of highly mobile hydrogen-related defects in Ref. [29]. The low value of the migration barriers indicates that the formation energy  $E_f$  of the hydrogen-related defects is the dominant term in the activation energy for self-diffusion, and that defect migration is not a rate-limiting step. These low barriers also confirm that for-

mation of hydrogen-related point defects can be treated as an equilibrium process, an assumption that underlies equation (3).

## Summary

We have applied first-principles computations based on density functional theory to the study of hydrogen-related point defects in  $\text{NaAlH}_4$ . The relevant point defects turn out to be positively or negatively charged, which has important repercussion for kinetics since the concentration of such defects will be heavily influenced by the presence of electrically active impurities in the material. In addition, some of the point defects produce large local deformations of the host lattice. Additional details can be found in Refs. [30] and [31].

## Acknowledgments

This work was supported by the University of California Energy Institute. Additional funding was provided by the Natural Sciences and Engineering Research Council of Canada (NSERC) and by DOE Award # DE-FG02-07ER46434. The work also made use of MRL Central Facilities supported by the NSF MRSEC Program under award No. DMR05-20415.

## References

- [1] L. Schlapbach and A. Züttel, “Hydrogen-storage materials for mobile applications”, *Nature* **414**, 353 (2001).
- [2] M. S. Dresselhaus and I. L. Thomas, “Alternative energy technologies”, *Nature* **414**, 332 (2001).
- [3] B. Bogdanovic and M. Schwickardi, “Ti-doped alkali metal aluminium hydrides as potential novel reversible hydrogen storage materials”, *J. Alloys Compd.* **253-254**, 1 (1997).
- [4] K. J. Gross, G. J. Thomas, and C. M. Jensen, “Catalyzed alanates for hydrogen storage”, *J. Alloys Compd.* **330-332**, 683 (2002).
- [5] G. J. Thomas, K. J., Gross, N. Y. C. Yang, and C. Jensen, “Microstructural characterization of catalyzed  $\text{NaAlH}_4$ ”, *J. Alloys Compd.* **330-332**, 702 (2002).
- [6] O. M. Løvvik and S. M. Opalka, “Density functional calculations of Ti-enhanced  $\text{NaAlH}_4$ ”, *Phys. Rev. B* **71**, 054103 1 (2005).
- [7] J. Graetz *et al.*, “X-ray absorption study of Ti-activated sodium aluminum hydride”, *Appl. Phys. Lett.* **85**, 500 (2004).
- [8] M. T. Kuba, S. S. Eaton, C. Morales, and C. M. Jensen, “Characterization of titanium dopants in sodium alanate by electron paramagnetic resonance spectroscopy”, *J. Mater. Res.* **20**, 3265 (2005).
- [9] M. Fichtner, P. Canton, O. Kircher and A. Leon, “Nanocrystalline alanates – Phase transformations, and catalysts”, *J. Alloys Compd.* **404-406**, 732 (2005).
- [10] D. Sun, T. Kiyobayashi, H. T. Takeshita, N. Kuriyama, and C. M. Jensen, “X-ray diffraction studies of titanium and zirconium doped  $\text{NaAlH}_4$ : elucidation of doping in-

duced structural changes and their relationship to enhanced hydrogen storage properties”, *J. Alloys Compd.* **337**, L8 (2002).

[11] J. Íñiguez, T. Yildirim, T. J. Udovic, M. Sulic, and C. M. Jensen, “Structure and hydrogen dynamics of pure and Ti-doped sodium alanate”, *Phys. Rev. B* **70**, 060101 1 (2004).

[12] F. A. Kroger, *The chemistry of imperfect crystals* (North-Holland Publishing Co., Amsterdam, 1964).

[13] C. G. Van de Walle, “Electronic materials theory: Interfaces and defects”, *J. Vac. Sci. Technol. A* **21**, S182 (2003).

[14] C. G. Van de Walle, “Defects and Impurities in Semiconductors”, in *Handbook of Materials Modeling*, edited by S. Yip (Springer, 2005), pp. 1877-1888.

[15] S. Gomes *et al.*, “Effects of milling and cycling of NaAlH<sub>4</sub> studied by vibrational spectroscopy and X-ray diffraction”, *J. Alloys Compd.* **390**, 305 (2005).

[16] H. W. Brinks *et al.*, “Synchrotron X-ray and neutron diffraction studies of NaAlH<sub>4</sub> containing Ti additives”, *J. Alloys Compd.* **376**, 215 (2004).

[17] E. H. Majzoub and K. J. Gross, “Titanium–halide catalyst-precursors in sodium aluminum hydrides”, *J. Alloys Compd.* **356-357**, 363 (2003).

[18] C. G. Van de Walle and J. Neugebauer, “First-principles calculations for defects and impurities: Applications to III-nitrides”, *J. Appl. Phys.* **95**, 3851 (2004).

[19] A. Peles and M.-Y. Chou, “Lattice dynamics and thermodynamic properties of NaAlH<sub>4</sub>: Density-functional calculations using a linear response theory”, *Phys. Rev. B* **73** 184302 (2006).

- [20] J. P. Perdew *et al.*, “Atoms, molecules, solids, and surfaces: applications of the generalized gradient approximation for exchange and correlations”, *Phys. Rev. B* **46**, 6671 (1992).
- [21] G. Kresse and J. Joubert, “From ultrasoft pseudopotentials to the projector augmented-wave method”, *Phys. Rev. B* **59**, 1758 (1999).
- [22] G. Kresse and J. Furthmüller, “Efficient iterative schemes for ab initio total-energy calculations using a plane-wave basis set”, *Phys. Rev. B* **54**, 11169 (1996).
- [23] A. Peles, J. A. Alford, Z. Ma, L. Yang, and M.-Y. Chou, “First-principles study of NaAlH<sub>4</sub> and Na<sub>3</sub>AlH<sub>6</sub> complex hydrides” *Phys. Rev. B* **70**, 165105 (2004).
- [24] G. Henkelman and H. Jónsson, “Improved tangent estimate in the nudged elastic band method for finding minimum energy paths and saddle points”, *J. Chem. Phys.* **113**, 9978 (2000).
- [25] P. W. Anderson, “Model for the Electronic Structure of Amorphous Semiconductors”, *Phys. Rev. Lett.* **34**, 953 (1975).
- [26] C. M. Jensen, R. Zidan, N. Mariels, A. Hee, and C. Hagen, *Int. J. Hydrogen Energy* **24** 461 (1999).
- [27] G. Sandrock, K. Gross, and G. Thomas, “Effect of Ti-catalyst content on the reversible hydrogen storage properties of the sodium alanates”, *J. Alloys Compd.* **339**, 299 (2002).
- [28] J. Wang, A. D. Ebner, R. Zidan, and J. A. Rittera, “Synergistic effects of co-dopants on the dehydrogenation kinetics of sodium aluminum hydride”, *J. Alloys Compd.* **391**, 245 (2005).

[29] O. Palumbo, R. Cantelli, A. Paolone, C. M. Jensen, and S. S. Srinivasan, “Motion of point defects and monitoring of chemical reactions in sodium aluminium hydride”, *J. Alloys Compd.* **404-406**, 748 (2005).

[30] A. Peles and C. G. Van de Walle, “Role of charged defects and impurities in kinetics of hydrogen storage materials: A first-principles study”, *Phys. Rev. B* **76**, 214101 (2007).

[31] C. G. Van de Walle, A. Peles, A. Janotti, and G. B. Wilson-Short, “Atomic and electronic structure of hydrogen-related centers in hydrogen storage materials” (to be published in *Physica B*).

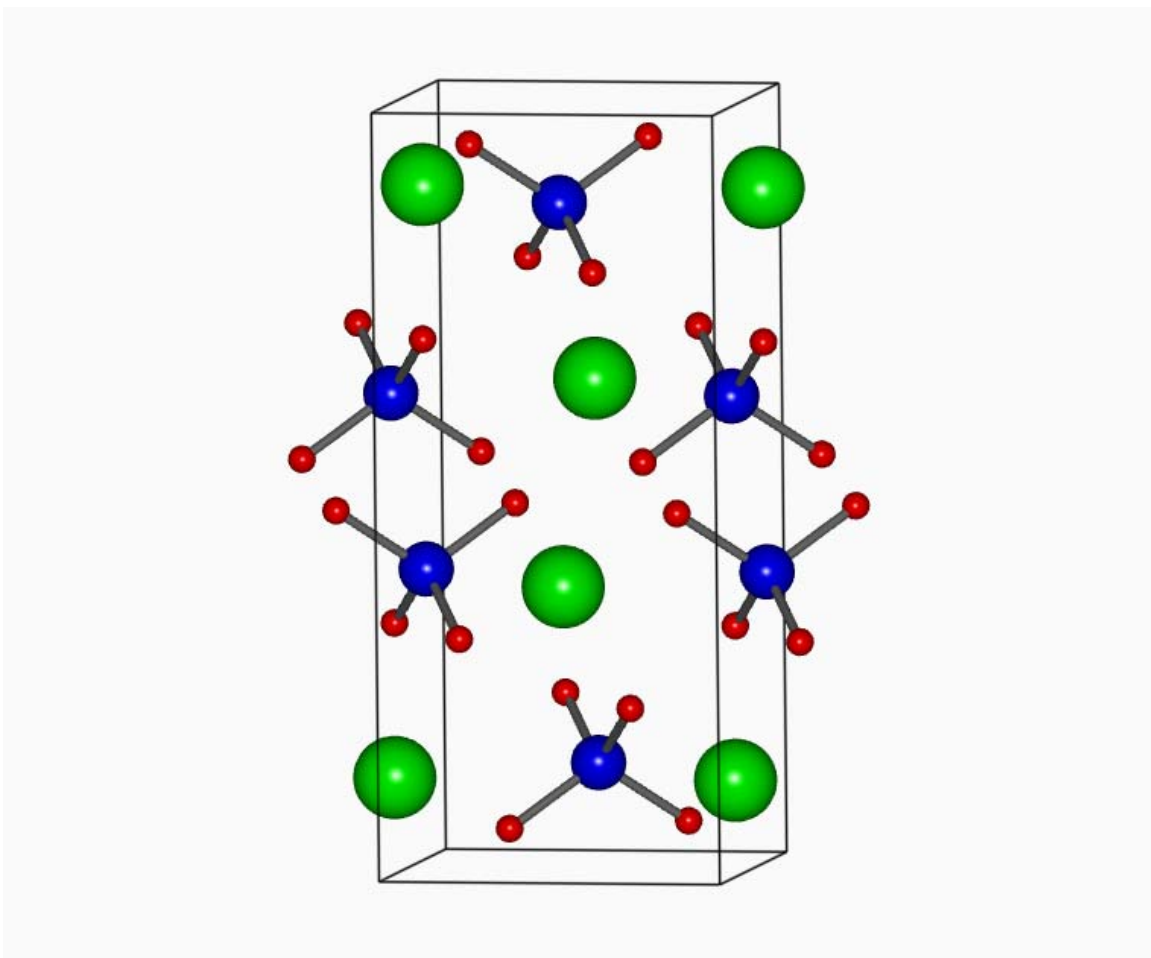


**Figure 1.** Schematic illustration of the atomic structure in a perfect NaAlH<sub>4</sub> crystal. The view is along the *a* axis, and the *c* axis of the crystal is along the vertical in the figure. Only one plane of Na and Al atoms is shown, along with the H atoms that are bonded to the Al. The boundaries of the tetrahedral supercell are indicated. Large green spheres are Na, medium blue spheres Al, and small red spheres H.

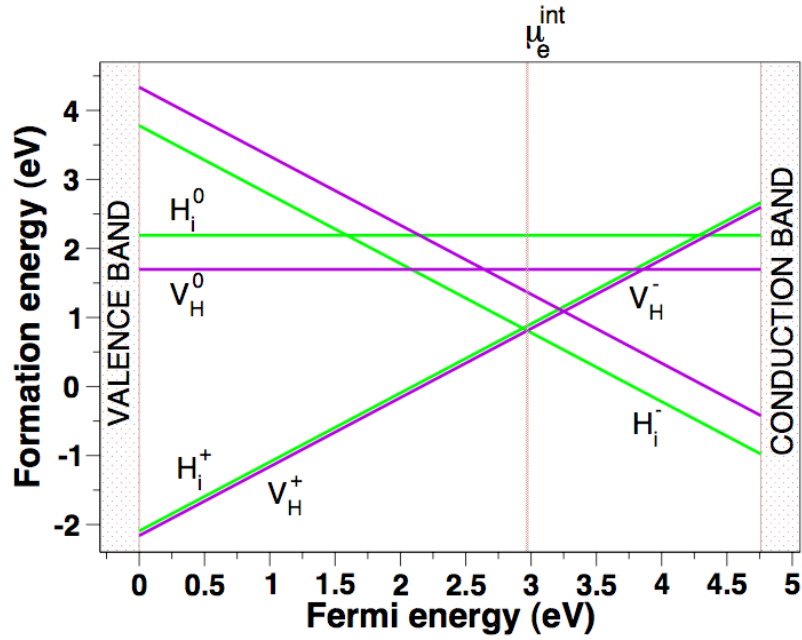


**Figure 2.** Calculated formation energies of relevant hydrogen-related defects in NaAlH<sub>4</sub> as a function of Fermi energy. The vertical line denotes the Fermi-level position determined by charge neutrality. Equilibrium with H<sub>2</sub> molecules at  $T=0$  is assumed.

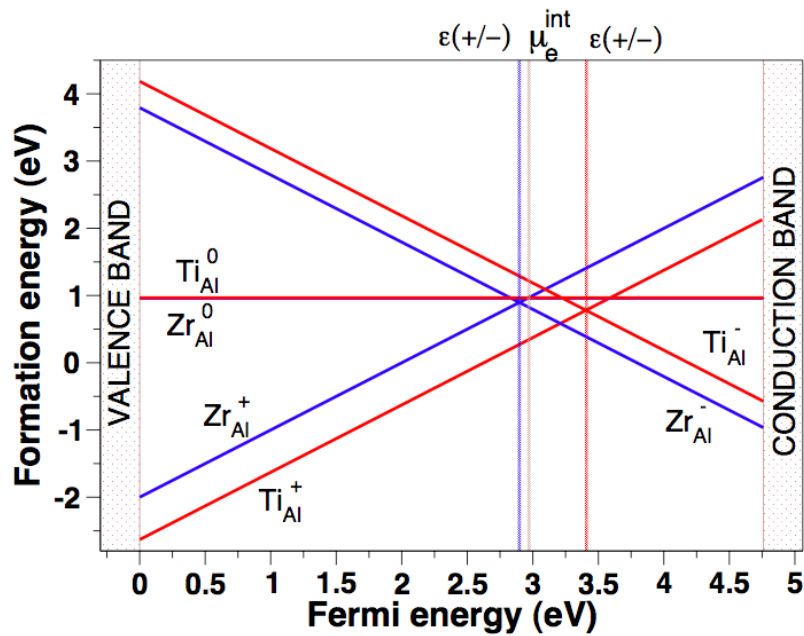


**Figure 3.** Calculated formation energies of selected impurities in NaAlH<sub>4</sub> as a function of Fermi energy. The vertical line denotes the Fermi-level position determined by charge neutrality, in the absence of other defects. Ti-related (red) and Zr-related (blue) defects are shown. For Ti and Zr, the chemical potentials were fixed to the energy of the bulk metals and Al-rich conditions were assumed.

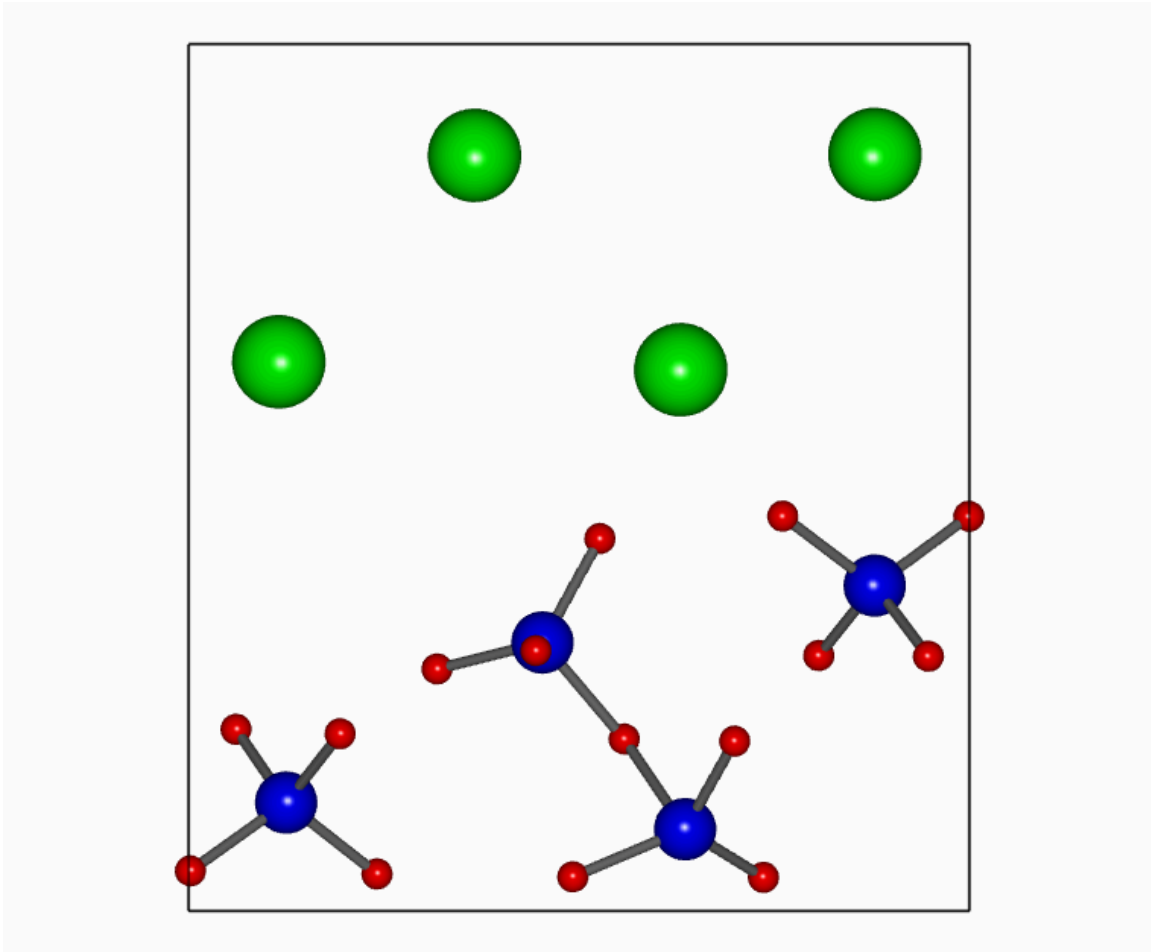


**Figure 4.** Schematic illustration of the atomic structure around a positively charged vacancy,  $V_{\text{H}}^+$ , in NaAlH<sub>4</sub>.

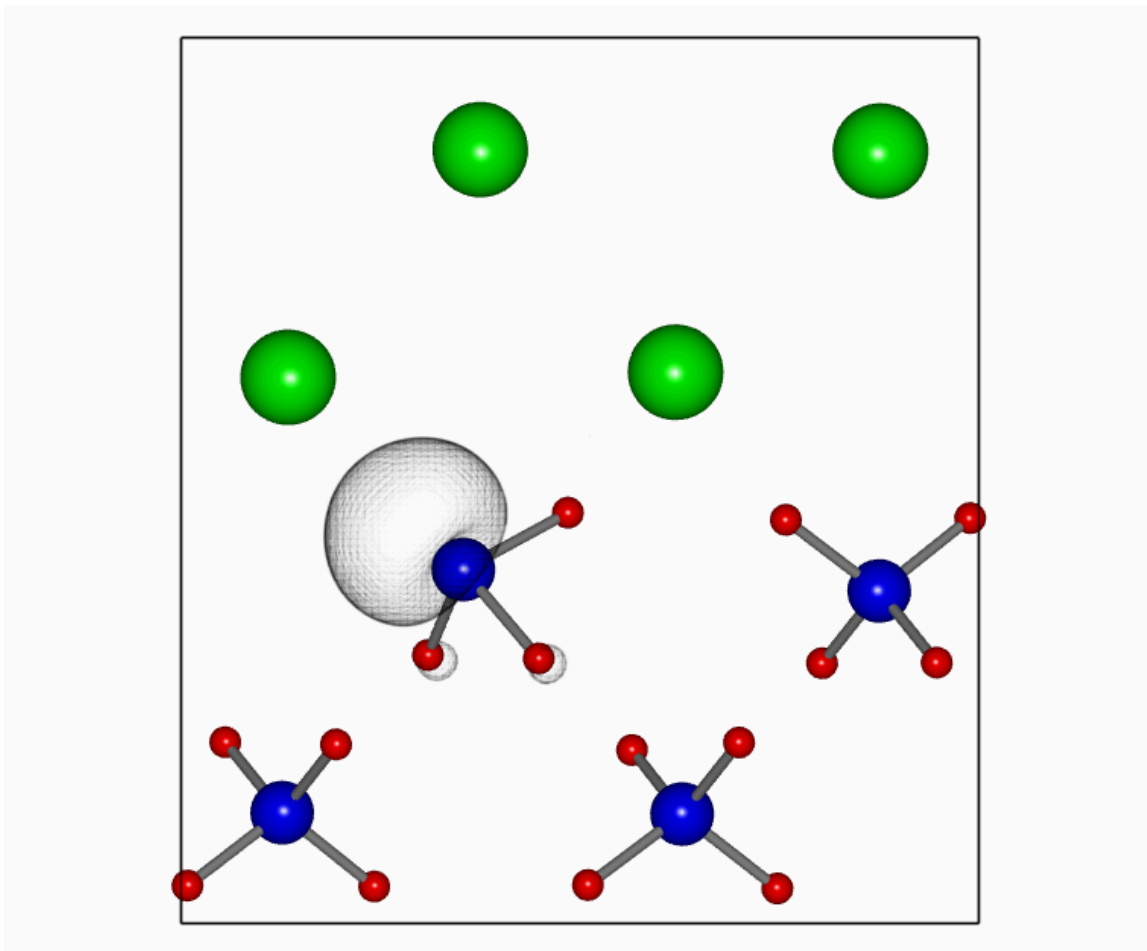


**Figure 5.** Schematic illustration of the atomic structure around a negatively charged vacancy,  $V_{\text{H}}^-$ , in  $\text{NaAlH}_4$ . An isosurface of the charge density associated with the defect state, which occurs at 2.5 eV above the valence-band maximum, is shown. The electron density at the isosurface is  $0.06 \text{ els}/\text{\AA}^3$ .

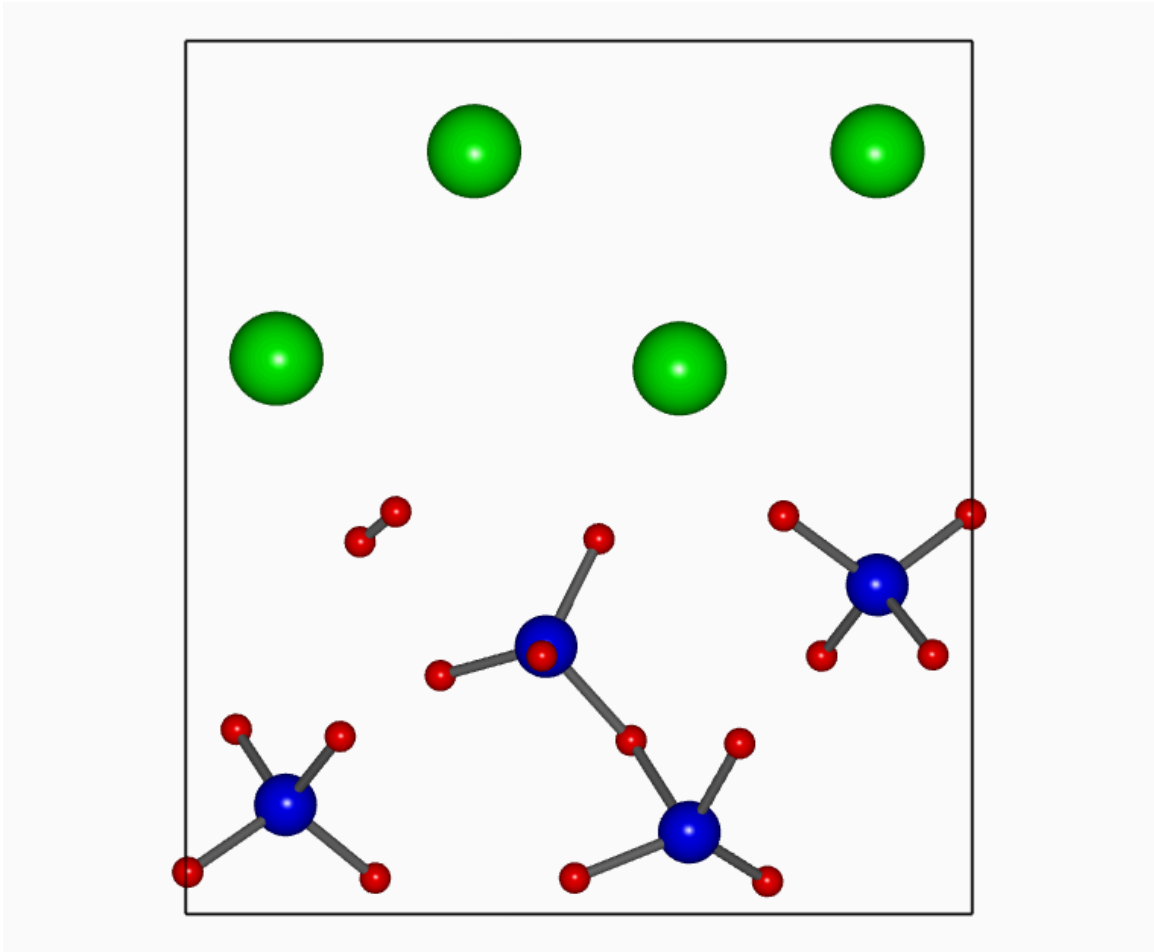


**Figure 6.** Schematic illustration of the atomic structure around a positively charged interstitial,  $H_i^+$ , in  $NaAlH_4$ .

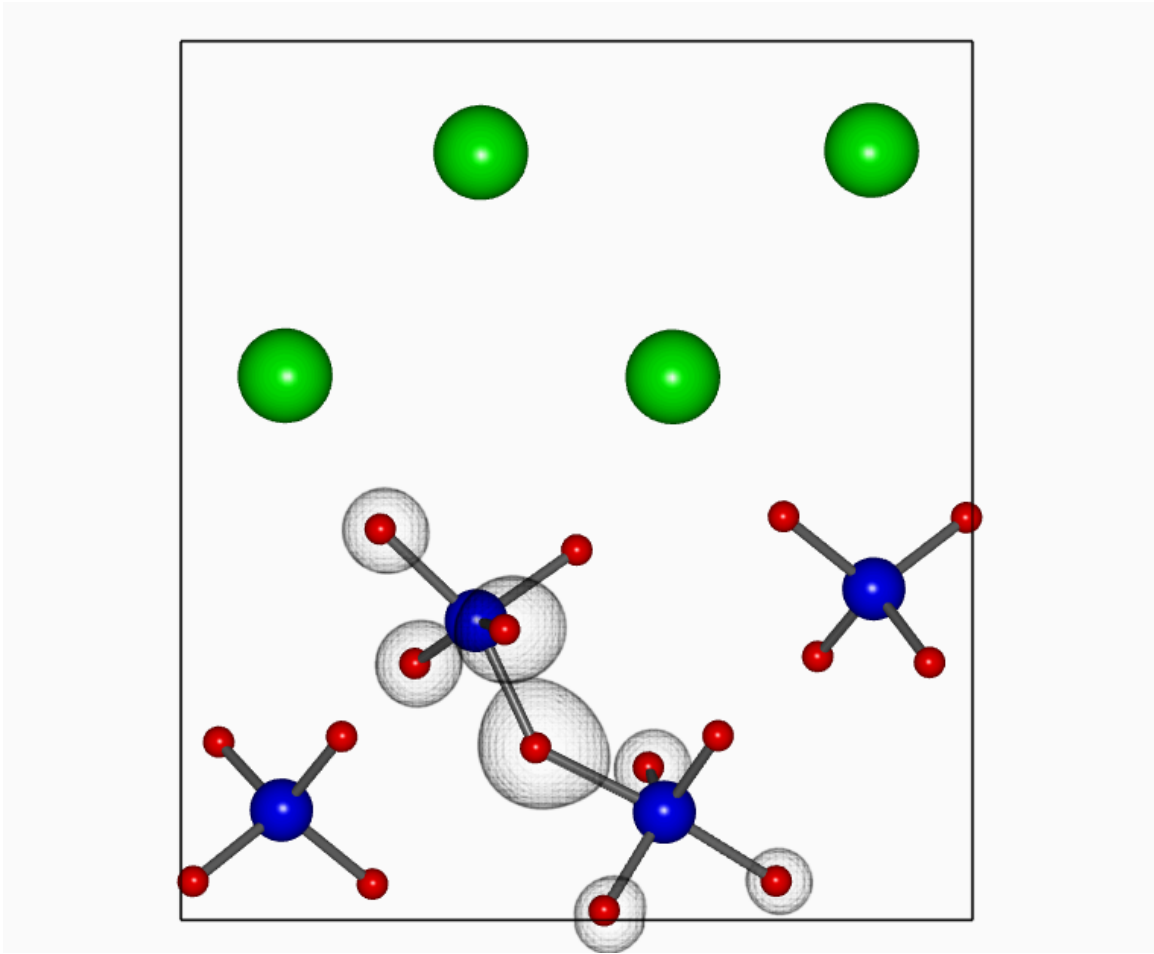


**Figure 7.** Schematic illustration of the atomic structure around a negatively charged interstitial,  $H_i^-$ , in  $NaAlH_4$ . An isosurface of the charge density associated with a defect state at 1.3 eV above the valence-band maximum is shown. The electron density at the isosurface is  $0.06 \text{ els}/\text{\AA}^3$ .